KIPS Trans. Softw. and Data Eng.
Vol.9, No.2 pp.69~76 pISSN: 2287-5905



https://doi.org/10.3745/KTSDE.2020.9.2.69

# Parametric Imaging with Respiratory Motion Correction for Contrast-Enhanced Ultrasonography

Ho-Joon Kim† · Yun-Seok Cho††

## ABSTRACT

In this paper, we introduce a method to visualize the contrast diffusion patterns and the dynamic vascular patterns in a contrast-enhanced ultrasound image sequence. We present an imaging technique to visualize parameters such as contrast arrival time, peak intensity time, and contrast decay time in contrast-enhanced ultrasound data. The contrast flow pattern and its velocity are important for characterizing focal liver lesions. We propose a method for representing the contrast diffusion patterns as an image. In the methods, respiratory motion may degrade the accuracy of the parametric images. Therefore, we present a respiratory motion tracking technique that uses dynamic weights and a momentum factor with respect to the respiration cycle. Through the experiment using 72 CEUS data sets, we show that the proposed method makes it possible to overcome the limitation of analysis by the naked eye and improves the reliability of the parametric images by compensating for respiratory motion in contrast-enhanced ultrasonography.

Keywords : Image Processing, Ultrasound Image, Parametric Imaging, Motion Tracking, Respiratory Motion

# 조영증강 초음파 진단에서 호흡에 의한 흔들림을 보정한 파라미터 영상 생성 기법

김 호 준† · 조 윤 석††

## 요 약

본 연구에서는 조영증강 초음파 영상에서 조영효과 확산 패턴과 동적 혈류 패턴을 가시화 하는 방법론을 제시한다. 세부적으로 조영증강 초음파 데이터에서 조영제의 전이시간, 최대 명도변화, 조영효과의 감쇄 시간 등과 같은 진단 파라미터를 영상으로 생성하는 기법을 제안한다. 간병변 진단과 같은 의료 진단에서 조영제의 전이와 확산 속도는 매우 중요한 요소가 된다. 이에 본 연구에서는 조영효과의 확산 패턴을 하나의 영상으로 표현하는 방법을 제시하였다. 이 과정에서 호흡에 의한 흔들림으로 인하여 영상의 정확도가 저하시키는 현상을 개선하기 위하여 호흡주기에 따른 동적 가중치와 모멘텀 요소를 사용하는 영상추적 기법을 제안하였다. 총 72개의 조영증강 데이터를 사용한 실험을 통하여, 제안된 기법이 초음파진단에서 육안 판별의 한계를 극복할 수 있게 하고, 호흡에 의한 흔들림을 보정함으로써 진단 파라미터의 신뢰도를 향상시킬 수 있음을 보인다.

키워드 : 영상 처리, 초음파 영상, 파라미터 영상생성, 모션 추적, 호흡에 의한 흔들림현상

## 1. Introduction

In recent years, researchers have reported that the assessment of perfusion using ultrasound contrast agents is beneficial in many diagnostic indications. Because of its non-invasive, non-irradiating and real-time imaging characteristics, contrast-enhanced ultrasonography (CEUS) has significantly improved diagnostic efficacy with respect to focal liver lesions [1-9]. Detection and characterization of focal liver lesions are presently the most common applications of CEUS. Liang et al. [1] proposed an automatic computation framework to assist clinicians in diagnosing Focal Liver Lesions (FLLs) in Contrast-Enhanced Ultrasound. Li et al. [3] investigated the use of CEUS with quantitative measurements to assess the stage of liver fibrosis in patients with chronic hepatitis B. They used the contrast arrival time (AT) and baseline intensity (BI) in hepatic artery, portal vein, hepatic vein, and liver parenchyma to calculate intrahepatic transit times, and analyzed the correlations between the quantitative parameters and the stages of fibrosis. Rognin et al. [4] proposed a parametric imaging technique as a diagnostic aid tool for characterizing lesion types. The

※ 본 연구는 과학기술정보통신부와 정보통신기술진흥센터의 소프웨어 중심대학 지원사업(2017-0-00130)의 지원을 받아 수행되었음.
† 종신회원 : 한동대학교 전산전자공학부 교수
†† 정 회 원 : 한동대학교 전산전자공학부 교수
Manuscript Received : June 19, 2019
First Revision : August 30, 2019
Accepted : August 31, 2019
* Corresponding Author : Ho-Joon Kim(hjkim@handong.edu)

vascular signatures are made conspicuous in a parametric imaging context by using a pixel classification method, whereby each pixel is categorized according to the polarity of its difference signal over time. Most medical imaging techniques, such as magnetic resonance imaging (MRI) or ultrasonography, suffer from respiratory motion artifacts, which lead to blurring and ghosting that significantly deteriorates the imaging quality [10-15]. Respiratory motion of the thorax complicates ultrasonographic detection of focal liver lesions. A number of solutions have been proposed to deal with the problem of respiratory motion. McClelland et al. [10] introduced a review of respiratory motion models and summarized and compared the different techniques used for a wide range of applications. Zhang et al. [11] proposed a combined approach of template matching and frame selection to correct the respiratory motion and improve the accuracy of the quantification evaluation of perfusion. Nakamoto et al. [12] proposed a method for intraoperative recovery of respiratory motion and deformation of the liver that uses laparoscopic freehand 3D ultrasound system. Mule et al. [13] developed an automatic respiratory gating method and tested it on CEUS hepatic data sets with focal lesions. In the common image-tracking and image registration techniques, various types of features are extracted from the pixel intensity and edge information [16-18]. However, because the micro-bubble effects in the CEUS image sequence cause individual pixel values to vary from frame to frame, the conventional object-tracking method may produce erroneous results for respiratory motion tracking.

In this paper, we introduce a method for visualizing the contrast diffusion patterns and the dynamic vascular patterns (DVP) in a CEUS image sequence. The underlying system is a diagnostic parameter visualization tool for characterizing focal liver lesions in CEUS. The system generates the parametric images that show the DVP data, the AT of contrast agents, and the blood flow patterns in focal liver lesions. We present an imaging technique for visualizing the AT, the peak intensity time (PT), and the decay time (DT) in CEUS data. For parametric imaging of the DVP, we introduce a modified version of Rognin's method [4]. In addition, we propose a way to represent the contrast diffusion patterns as an image. To solve the respiratory motion problem, we propose a motion tracking technique that uses dynamic weights and a momentum factor with respect to the respiration cycle, and we define a weight-updating rule and an image-tracking method. Through the experiments using a set of clinical data, we show that the proposed methods can improve the reliability of the parametric image data by compensating for the respiratory motion in ultrasonography.

## 2. Background

Underlying our method is a parameter visualization system for contrast-enhanced ultrasonography. As shown in Fig. 1, the system consists of three modules: a preprocessing module, a motion-tracking module, and a parametric imaging module. The preprocessing module removes abnormal frames by analyzing the consistency between consecutive frames. This is followed by a respiration cycle detection process and then the motion-tracking module, for which we propose an image tracking method. In the parametric imaging module, the diagnostic parameters are extracted from the time-intensity curve (TIC) analysis process, and visualized as image data. The module generates not only DVP parametric images, which include the data for peak intensity time (PT) and DT, but also the AT images and diffusion pattern images.

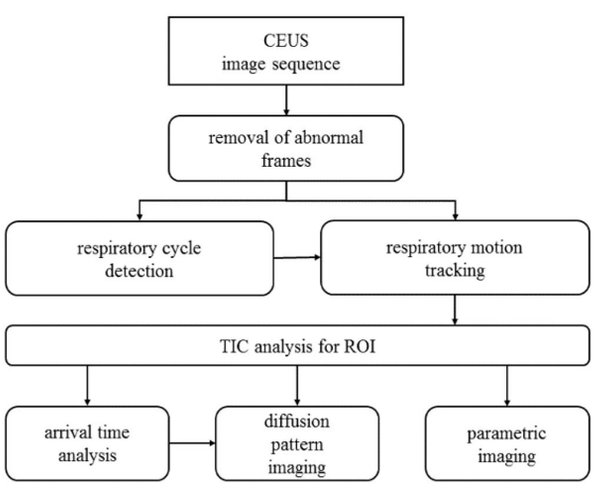


Fig. 1. The Structure of the Parameter Visualization System that Underlies Our Method

## 3. Visualization of Diagnostic Parameters in a CEUS Image Sequence

### 3.1 Arrival Time Imaging

The time-intensity curve of an arbitrary region of interest (ROI) in typical CEUS data is shown in Fig. 2. To extract various parameters to diagnose liver disease, we first extract a smoothed curve from the raw data of the ROI and then a fitted curve is generated to remove the local maxima and

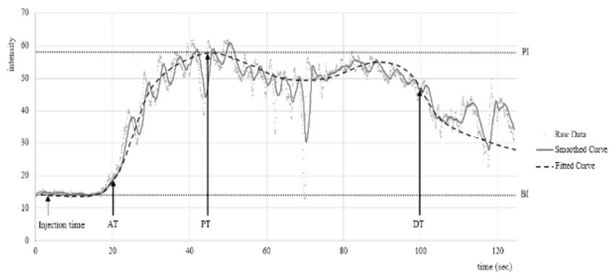


Fig. 2. The Time-Intensity Curve of a Typical CEUS Image and the Extracted Parameters

minima in the curve. As seen in the figure, the system automatically extracts a set of basic quantitative parameters, including baseline intensity (BI), peak intensity (PI). The AT is the time at which the intensity value exceeds the BI by a specified rate, e.g., 10%; the PT is the time at which the intensity reaches its peak; and And the DT is the time at which the intensity is decreased from the PI by a specific rate, e.g., 20%.

These extracted parameters can be utilized for the detection and characterization of focal liver lesions [2-4, 7]. In this paper, we introduce a method for visualizing more refined information from these parameters. We have developed an arrival time imaging technique by which the relative arrival time is represented as a pixel value:

$$A_i = \frac{T_i - T_{min}}{T_{max} - T_{min}}, \tag{1}$$

where $\mathbf{A_i}$ is the relative arrival time, $\mathbf{T_i}$ is the arrival time of pixel $\mathbf{i}$, and $\mathbf{T_{min}}$ and $\mathbf{T_{max}}$ are the earliest and the latest arrival time of the signals, respectively. The pixel value is determined from the relative arrival time as an RGB color value $\mathbf{x_i}$= ($\mathbf{x_i^R}$,$\mathbf{x_i^G}$,$\mathbf{x_i^B}$), where

$$x_i^R = \begin{cases} 255 & if\ (0 \le A_i \le 0.5) \\ 2 \cdot (1 - A_i) \cdot 255 & if\ (0.5 < A_i \le 1.0) \end{cases} \tag{2}$$

$$x_i^G = \begin{cases} 2 \cdot A_i \cdot 255 & if\ (0 \le A_i \le 0.5) \\ 255 & if\ (0.5 < A_i \le 1.0) \end{cases} \tag{3}$$

$$x_i^B = \begin{cases} 0 & if\ (0 \le A_i \le 0.5) \\ 2 \cdot (A_i - 0.5) \cdot 255 & if\ (0.5 < A_i \le 1.0). \end{cases} \tag{4}$$

The earliest arrival time is represented as pure red; the pixel value gradually changes from the red to yellow to cyan in proportion to the arrival time. With this method, a dynamic arrival pattern in CEUS image sequence is represented as a static image pattern. This visualization technique is helpful in analyzing the relative arrival time of each pixel and the flow pattern of contrast agents in the ROI. However, when the distribution of arrival times in the image is very unbalanced distribution of arrival time, it may be difficult to identify the arrival pattern with the naked eye. As an optional function, we added a post processing using a histogram equalization process.

### 3.2 Parametric Imaging

In contrast-enhanced ultrasound data, the differentiation between hyper-enhanced and hypo-enhanced signatures plays an important role in the diagnosis of focal liver lesions. Rognin et al. [4] proposed a DVP parametric imaging method as a diagnostic aid tool in which each pixel in the ROI is classified into one of four categories: unipolar positive, unipolar negative, bipolar positive-negative and bipolar negative-positive. In this paper, we introduce a modified version of Rognin's method for parametric imaging, where the difference between the TICs of the ROI and its adjacent parenchyma is calculated as

$$d_i(t) = (f_i(t) - b_i) - (f_{ref}(t) - b_{ref}) \tag{5}$$

where $f_i(t)$ and $f_{ref}(t)$ are the intensity of pixel $i$ and the average intensity of the reference region, respectively, and $b_i$ and $b_{ref}$ are the BI of pixel $i$ and the average BI of the reference region, respectively. To determine the polarity of the signal, we adopted the following rule:

$$\begin{cases} If\ (\frac{D_i^+}{D_i^-} > \theta) & : unipolar+, \\ If\ (\frac{D_i^-}{D_i^+} > \theta) & : unipolar-, \\ Otherwise, & : bipolar. \end{cases}$$

In the rule, $\theta$ is a threshold value used to determine the polarity of the signal and $D_i^+$ and $D_i^-$ are calculated as

$$D_i^+ = \sum_{t=T_s\ (d_i>0)}^{T_e} d_i(t), \tag{6}$$

$$D_i^- = -\sum_{t=T_s\ (d_i<0)}^{T_e} d_i(t), \tag{7}$$

where $T_s$ and $T_e$ are the first and the last frame of the image sequence, respectively. When the signal is bipolar, the bipolar type and the intensity value of the pixel are calculated. For this situation, we defined a median time $T_m$ as

$$T_m = \underset{T_k}{\operatorname{argmax}} \left( \left| \sum_{t=T_s}^{T_k} d_i(t) - \sum_{t=T_{k+1}}^{T_e} d_i(t) \right| \right) \tag{8}$$

The following rule is used to determine the polarity type of the signal at pixel $i$:

$$if\left(\left(\sum_{t=T_s}^{T_m} d_i(t) - \sum_{t=T_{m+1}}^{T_e} d_i(t)\right) > 0\right)$$
$$\text{then } hyper-enhancement\ followed\ by\ hypo-enhancement,$$
$$else\ hypo-enhancement\ followed\ by\ hyper-enhancement.$$

After the classification process, the pixel value, $x_i = (x_i^R, x_i^G, x_i^B)$, is calculated using the following rules:

*Case 1: Unipolar positive (hyper-enhanced)*

$$\begin{cases} x_i^R = 0 \\ x_i^G = \left(\dfrac{D_i^+ - D_i^-}{D_{max}}\right) \cdot 255 \\ x_i^B = 0 \end{cases}$$

*Case 2: Unipolar negative (hypo-enhanced)*

$$\begin{cases} x_i^R = 0 \\ x_i^G = 0 \\ x_i^B = \left(\dfrac{D_i^- - D_i^+}{D_{max}}\right) \cdot 255 \end{cases}$$

*Case 3: Bipolar positive − negative (hyper-enhanced followed by hypo-enhanced)*

$$\begin{cases} x_i^R = \left(\dfrac{\sum_{t=T_s}^{T_m} d_i(t) - \sum_{t=T_{m+1}}^{T_e} d_i(t)}{D_{max}}\right) \cdot 255 \\ x_i^G = 0 \\ x_i^B = 0 \end{cases}$$

*Case 4: Bipolar negative - positive (hypo-enhanced followed by hyper-enhanced)*

$$\begin{cases} x_i^R = \left(\dfrac{\sum_{t=T_{m+1}}^{T_e} d_i(t) - \sum_{t=T_s}^{T_m} d_i(t)}{D_{max}}\right) \cdot 255 \\ x_i^G = \left(\dfrac{\sum_{t=T_{m+1}}^{T_e} d_i(t) - \sum_{t=T_s}^{T_m} d_i(t)}{D_{max}}\right) \cdot 255 \\ x_i^B = 0 \end{cases}$$

In the above rules,

$$D_{max} = \max_i\left(\sum_{t=T_s}^{T_e} |d_i(t)|\right). \quad (9)$$

### 3.3 Diffusion Pattern Imaging

The contrast flow pattern in the CEUS data is used to characterize a focalliver lesion. During the diffusion period, i.e., the period between the arrival time and the peak intensity time, the flow pattern of the contrast agent provides data on blood flow, the shape of the blood vessels, and density changes. However, it is difficult to discern the information from the CEUS images with the naked eye because it is fast and minute. Therefore, we propose a visualization method in which the time-based contrast diffusion pattern is represented by the arrows and numbers in the image. Wedivide the diffusion period into a specific number (e.g., 20) of stages, each the same length of time. For each location in the ROI, the stage number of its arrival time is marked on the image, for every two consecutive stages, if a transition from a location to its adjacent location is found, the direction is marked with an arrow. Fig. 3 illustrates the diffusion pattern image, where the arrow and the number are the direction of the contrast flow and the relative arrival time, respectively. The background is the gray-scale image of the arrival time data.

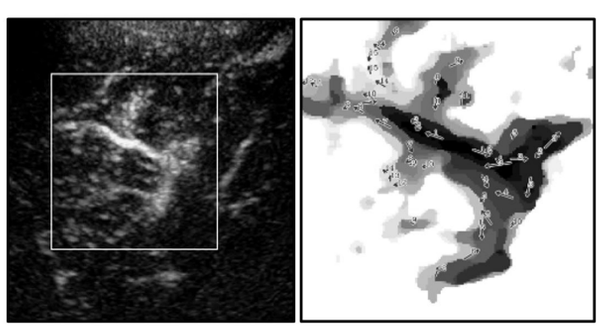

(a) (b)

Fig. 3. An Illustration of the Diffusion Pattern Image: (a) Input Data and ROI and (b) Diffusion Pattern Image for the ROI

## 4. Respiratory Motion Tracking and Compensation

Respiratory motion distorts the signals in most ultra-sonographic images. Moreover, CEUS image is accompanied by the noise in the form of blinking regions caused by micro-bubble contrast agents. Fig. 4 illustrates the change in the location of ROI in the CEUS image sequence. Whena fixed ROI is established for data analysis, it sometimes is displaced from the desired location due to the respiratory motion because of respiratory motion. To solve this problem, we propose a respiratory motion tracking technique to use with CEUS data.

The tracking method is a similarity-based algorithm in which the similarity measure, defined by Eq. (10), is applied to the image-matching process.

$$S(X^{t1}, X^{t2}, k) = \frac{1}{N}\sum_{i \in ROI}(1 - |x_i^{t1}(0) - x_i^{t2}(k)|) \quad (10)$$

$X^t$ is the image data at time $t$, the constant $N$ is the

number of pixels in the ROI. $x_i$ is the intensity of pixel $i$, and $k$ is the relative location in the 120-neighborhood of the pixel. The tracking method finds a direction code for the given frame. As shown in Eq. (11), the direction code is selected as one of the 121 locations so that it has the maximum similarity measurement value.

$$v^t = \underset{k\in\{0,1,..,120\}}{argmax}\ (w_k^t \cdot S(X^t, X^{t+1}, k)), \tag{11}$$

where a time dependant variable $w_k^t$ is the dynamic weight value for the relative location $k$.

One problem with the motion-tracking process based on image similarity is the noise effect due to the blinking of the micro-bubble agent in the CEUS data. We analyzed the average noise ratio for 60 typical CEUS data sets and found that it increases in proportion to the contrast agent's density. Because this noise may degrade the accuracy of the similarity measure, we suggest the use of a dynamic weight that reflects the momentum factor in the tracking process. In Eq. (11), the weight $w_k^t$ is dynamically updated by Eqs. (12), (13) and (14):

$$w_k^t = w_k^{t-1} + \Delta w_k^t, \tag{12}$$

$$\Delta w_k^t = \begin{cases} R(t)\cdot(\alpha - d(v^{t-1}, k)) & if\ d(v^{t-1}, k) < \beta \\ 1.0 - w_k^{t-1} & otherwise \end{cases} \tag{13}$$

and

$$R(t) = \gamma \cdot sin\left(\frac{(t-t_0)\pi}{\tau}\right). \tag{14}$$

$\alpha$ is the maximum distance between two arbitrary pixels in the 120-neighborhood, $\beta$ is a threshold value that determines whether the weight will increase or decrease, $R(t)$ is the momentum factor of the respiratory motion, $d(v^{t-1}, k)$ is the Euclidean distance between two relative-location points $v^{t-1}$ and $k$, $t_0$ is the start time of the current respiration cycle, $\tau$ is the estimated length of the respiration cycle, and $\gamma$ is a constant in the range [0, 1.0]. Therefore, the weight change $\Delta w_k^t$ is inversely proportional to the difference between the current location and the previous location and is directly proportional to the sine function of the respiration cycle.

## 5. Experimental Results

A total of 72 contrast-enhanced ultrasound data sets were used in the evaluation of the proposed methods' performance in characterizing focal liver lesions. We used the Keras environment running on a PC with an Intel(R) Core(TM) i7-6850 CPU (3.60 GHz; Intel Corp., Santa Clara, CA, USA) and an Nvidia GeForce 1080 Ti GPU (Nvidia, Santa Clara, CA, USA).

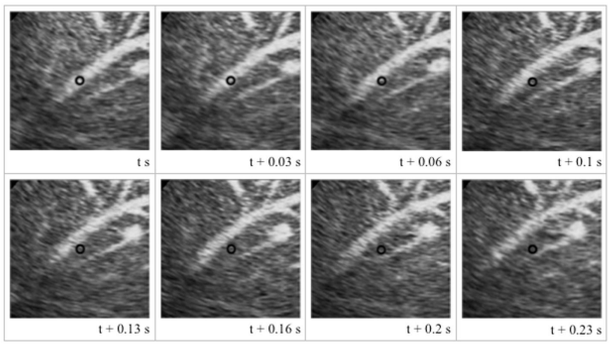


Fig. 4. An Example of the ROI Using a Fixed Location in the Image

Fig. 5-7 show the experimental results of the parameter visualization technique. Fig. 5 shows examples of AT images. Fig. 5(a) is an image frame captured from the CEUS data and ROI; Fig. 5(b) and 5(c) are the AT images of the image frame with gray scale and color value, respectively; and Fig. 5(d) is the result of histogram equalization result of the image in Fig. 5(c). The red and cyan pixels represent the early and late ATs, respectively. We can easily recognize the arrival pattern of the signal from the images.

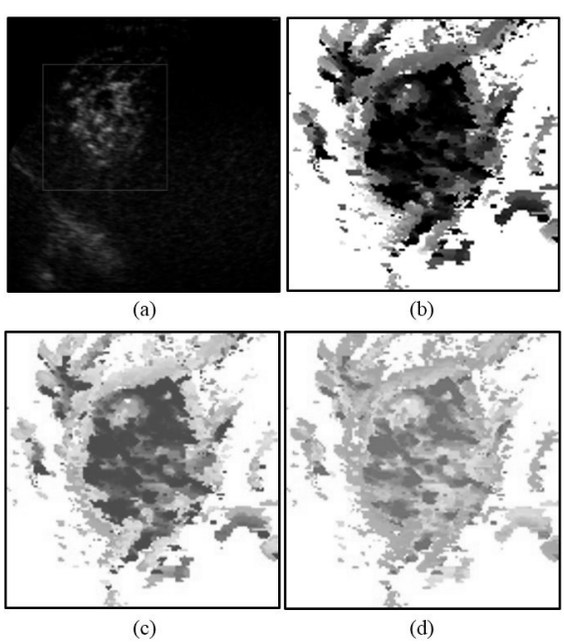


Fig. 5. Examples of Arrival Time (AT) Images. (a) Input Data and ROI, (b) AT Image (Gray Scale), (c) AT Image (Color), and (d) the Result of Histogram Equalization

Fig. 6 compares the images of the parameters AT(b), PT(c), and DT(d) for the same ROI shown in Fig. 6(a). The parameters, and thus the images, have relatively different values, hence, they can be used to characterize liver lesions.

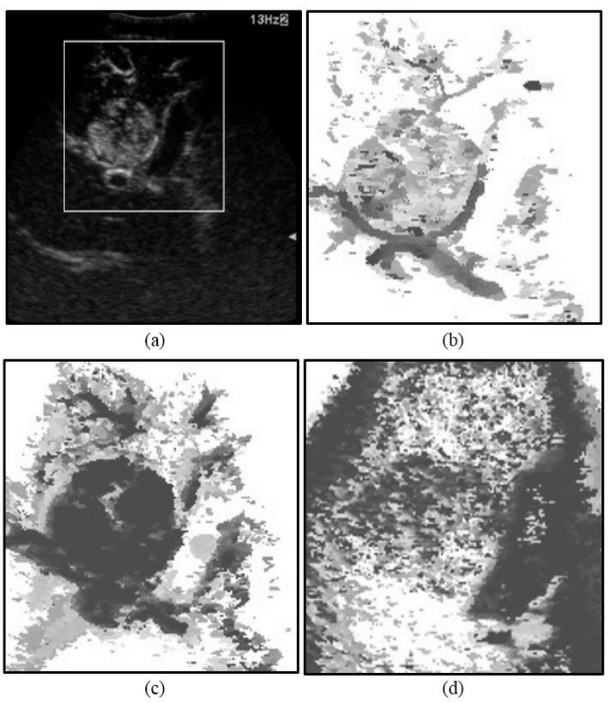


Fig. 6. Examples of Parameter Visualization: (a) Input Data and ROI, (b) Arrival Time (AT) Image, (c) Peak Intensity Time (PT) Image, and (d) Decay Time (DT) Image

Fig. 7 is an illustration of the diffusion pattern image, which provides more detailed information about the arrival pattern of contrast agents. The direction of blood flow and the relative AT of contrast agents are indicated by arrows and numbers on the image.

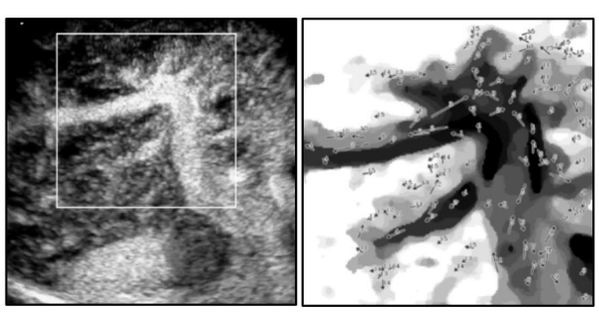


Fig. 7. An Example of a Diffusion Pattern Image: (a) Input Data and ROI and (b) the Diffusion Pattern Image for the ROI

We implemented the parametric imaging technique described in the previous sections. As seen in Fig. 8, each pixel in the ROI is classified into one of four classes, and its value is determined. In Fig. 8(b), the green and blue pixels are the unipolar positive and negative signals, respectively, the red pixels are hyper-enhancement followed by hypo-enhancement signatures, and the yellow pixels are hypo-enhancement followed by hyper-enhancement signatures. This image helps to characterize the liver lesions using CEUS. For example, thecolor of a pixel or a region in the image is used to differentiate between benign and malignant focal liver lesions.

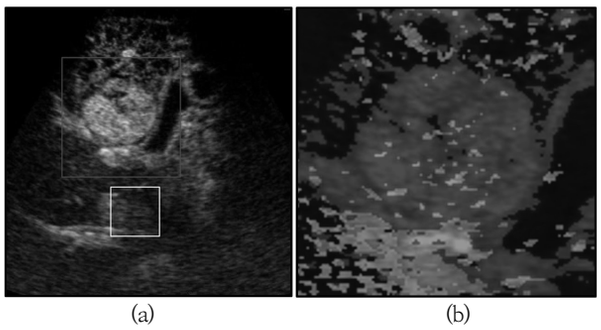


Fig. 8. An Example of the Parametric Image Using the Proposed Method: (a) ROI and Reference Region and (b) the Parametric Image of the ROI

As discussed in the previous section, respiratory motion periodicallychanges the location of the ROI in the CEUS image sequence. An ROI with fixed x and y coordinates in the image plane is frequently dislodged from its original location due to respiratory motion. The proposed motion-tracking algorithm consistently adjusts the location of the ROI to the desired location. Fig. 9 shows results of compensating for respiratory motion. The dashed-line circles indicate the fixed position of the ROI and the solid-line circles indicate the position of the ROI adjusted by the proposed method. The results show that the motion-tracking process makes it possible to retain the desired original location of ROI.

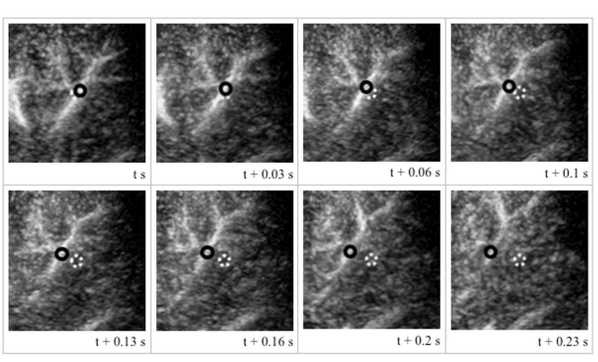


Fig. 9. An Example of Respiratory Motion Tracking and Compensation; The Fixed ROI (Dashed-Line Circle) and the Corrected ROI (Solid-Line Circle)

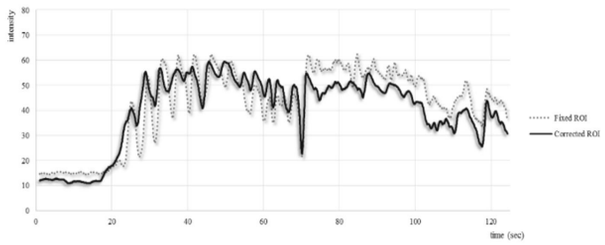


Fig. 10. A Time-Intensity Curve (TIC) with the Respiratory Motion Correction; TIC for the Fixed ROI (Dashed Line) and TIC for the Corrected ROI (Solid Line)

Fig. 10 shows that the respiratory motion correction process using the proposed tracking algorithm can reduce the erroneous variations on the TICs.

The AT image provides meaningful information such as blood flow and the diffusion pattern of contrast agents for the characterization of a focal liver mass. However, the ROI may move from its original location due to respiratory motion during the measurement process, causing distortion of the contour in the mass image. Our method can overcome this problem. Fig. 11 (a) is a sample image from the CEUS image sequence used to detect the liver mass. While the AT image without motion compensation has a blurred and distorted boundary contour [Fig. 11(b)], the motion-compensated image preserves the original shape of contour [Fig. 11(c) and Fig. 11(d)]. Thus, a more accurate shape of the liver mass is extracted by the proposed technique.

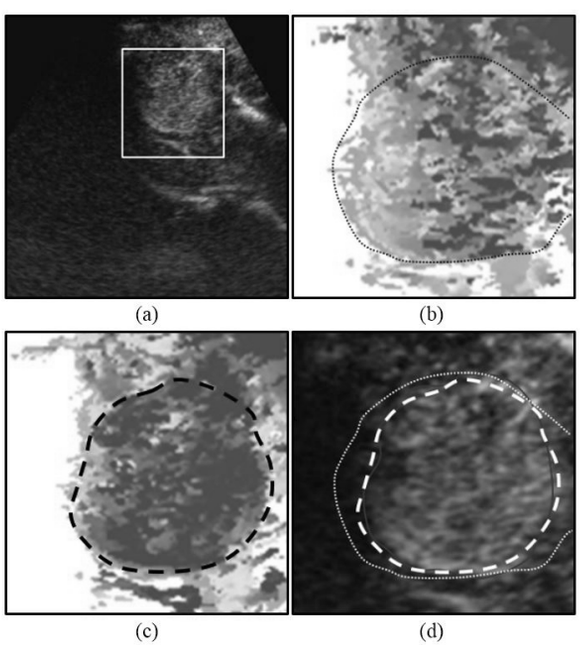


Fig. 11. (a) The Mass Image in a Sampled Frame, (b) the Arrival Time (AT) Image before Motion Compensation, (c) the AT Image after the Compensation, and (d) Comparison of the Contours Extracted from the Two Images and the Real Contour

## 6. Conclusions

The presented parameter visualization and respiratory motion tracking techniques can be used to analyze contrast-enhanced ultrasonographic images, where the AT, PT, and DT of contrast agents play important roles in the detection and characterization of focal liver lesions. In addition, the AT data is used to derive a contrast diffusion pattern image with flow direction arrows. Dynamic weight and its updating rule are proposed for respiratory motion tracking and correction. The efficacy of the proposed methods was evaluated using data from 72 CEUS data sets. The results showed that the respiratory motion correction technique can improve the accuracy of the parametric imaging process, and the parameter visualization methods can help overcome the limitation of the naked eye when analyzing CEUS data.

## References

[1] X. Liang, Q. Cao, R. Huang, and L. Lin, "Reconizing focal liver lesions in contrast-enhanced ultrasound with discriminatively trained spatio-temporal model," arXiv:1502.007540v1[cs.CV] 3 Feb. 2015.

[2] X. Ma, W. Ling, F. Xia, Y. Zhang, C. Zhu, and J. He, "Application of Contrast-Enhanced Ultrasound(CUES) in lymphomatous lymph nodes: a comparison between PET/CT and Contrast-Enhanced CT," *Contrast Media & Molecular Imaging*, Vol.2019, article ID 5709698, https://doi.org/10.1155/2019/5709698, 2019.

[3] N. Li, H. Ding, P. Fan, X. Lin, C. Xu, W. Wang, X. Xu, and J. Wang, " Intrahepatic transit time predicts liver fibrosis in patients with chronic hepatitis B: quantitative assessment with contrast-enhanced ultrasonography," *Ultrasound in Medicine and Biology*, Vol.36, No.7, pp.1066-1075, 2010.

[4] N. Rognin, M. Arditi, L. Mercier, J. Peter, A. Frinking, M. Schneider, G. Perrenoud, A. Anaye, J. Meuwly, and F. Tranquart, "Parametric imaging for characterizing focal liver lesions in contrast-enhanced ultrasound," *IEEE Transaction on Ultrasonics, Ferroelectrics, and Frequency Control*. Vol.57, No.11, pp.2503-2511, 2010.

[5] R. Iezzi, G. Petrone, A. Ferrante, L. Lauriola, G. Vincenzoni, M. F. la Torre, F. Snider, G. Rindi, and L. Bonomo, "The role of contrast-enhanced ultrasound (CEUS) in visualizing atherosclerotic carotid plaque vulnerability: Which injection protocol? Which scanning technique," *European Journal*

*of Radiology*, Vol.84, No.1, pp.865-871, 2015.

[6] L. Chiorean, V. Cantisani, C. Jenssen, P. S. Sidhu, U. Baum, and C. F. Dietrich, "Focal masses in a non-cirrhotic liver: The additional benefit of CEUS over baseline imaging," *European Journal of Radiology*, Vol.84, No.1, pp.1636-1643, 2015.

[7] A. Lim, S. Taylor-Robinson, N Patel, R. Eckersley, R. Goldin, G Hamilton, G. Foster, H. Thomas, D. Cosgrove, and M. Blomley, "Hepatic vein transit times using a microbubble agent can predict disease severity non-invasively in patients with hepatitis C," *Gut 2005*, Vol.54, No.1, pp.128-133, 2005.

[8] S. Wilson and P. Burns, "An algorithm for the diagnosis of focal liver masses using microbubble contrast-enhanced pulse-inversion sonography," *American Journal of Roentgenology,* Vol.186, No.1, pp.1401-1411, 2006.

[9] C. Dietrich, "Characterisation of focal liver lesions with contrast enhanced ultrasonography," *European Journal of Radiology*, Vol.10, No.11, pp.9-17, 2003.

[10] J. McClelland, D. Hawkes, T. Schaeffter, and A. King, "Respiratory motion models: a review," *Medical Image Analysis*, Vol.17, No.1, pp.19-42, 2013.

[11] J. Zhang, M. Din, F. Meng, M. Yuchi, and X. Zhang, "Respiratory motion correction in free-breathing ultrasound image sequence for quantification of hepatic perfusion," *Medical Physics*, Vol.38, No.1, pp.4737-4748, 2011.

[12] M. Nakamoto, H. Hirayama, Y. Sato, K. Konishi, Y. Kakeji, M. Hashizume, and S. Tamura, "Recovery of respiratory motion and deformation of the liver using laparoscopic freehand 3d ultrasound system," *Medical Image Analysis*, Vol.11, No.5, pp.429-442, 2007.

[13] S. Mule, N. Kachenoura, O. Lucidarme, A. Oliverira, C. Pellot-Barakat, A. Herment, and F. Frouin, "An automatic respiratory gating method for the improvement of micro-circulation evaluation: application to contrast-enhanced ultrasound studies of focal liver lesions," *Physics in Medicine and Biology*, Vol.56, No.1, pp.5153-5165, 2011.

[14] V. Hamy, N. Dikaios, S. Punwani, A. Melbourne, A. Latifoltojar, J. Makanyanga, M. Chouhan, E. Helbren, A. Menys, S. Taylor, D. Atkinson, "Respiratory motion correction in dynamic MRI using robust data decomposition registration-Application to DCE-MRI," *Medical Image Analysis*, Vol.18, No.2, pp.301-313, 2014.

[15] W. Jiang, Z. Liu, K.-H. Lee, S. Chen, Y.-L. Ng, Q. Dou, H.-C. Chang, and K.-W. Kwok, "Respiratory motion correction in abdomical MRI using a densely connected U-Net with GAN-guided training," arxiv:2906.09745, 2019.

[16] J. Gance, T. Dewez, and J. Travelletti, "Target detection and tracking of moving objects for characterizing landslide displacement from time-lapse terrestrial optical image," *Engineering Geology*, Vol.172, No.1, pp.26-40, 2014.

[17] X. Qian, L. Han, and Y. Cheng, "An object tracking method based on local matting for night fusion image," *Infrared Physics & Technology*, Vol.67, No.1, pp.455-461, 2014.

[18] J. Yan, F. Wang , X. Cao, and J. Zhang , "Robust object tracking using least absolute deviation," *Image and Vision Computing*, Vol.32, No.1, pp.930-939, 2014.

**Ho-Joon Kim**

https://orcid.org/0000-0002-8951-8441
e-mail : hjkim@handong.edu

He is a professor at the school of Computer Science and Electrical Engineering in Handong Global University since 1996. He received Ph.D. from in Computer Science from Korea Advanced Institute of Science and Technology (KAIST) in 1995. His research interests include image processing, pattern recognition, medical data analysis, machine learning and computer vision.

**Yun-Seok Cho**

https://orcid.org/0000-0002-7166-6390
e-mail : yscho@handong.edu

He is a professor at the school of Computer Science and Electrical Engineering in Handong Global University since 1995. He received Ph.D. from in Electrical Engineering from Korea Advanced Institute of Science and Technology (KAIST) in 1994. His research areas include digital signal processing, embedded system, Internet of Things, and Web and mobile integration platform.